Polarization shaping of few-cycle terahertz waves

Kanghee Lee,[1] **Minwoo Yi,**[1] **Jin Dong Song,**[2] **and Jaewook Ahn**[1,*]

[1]*Department of Physics, KAIST, Daejeon 305-701, Korea*
[2]*Nano Photonics Research Center, Korea Institute of Science and Technology, Seoul 136-791, Korea*
[*]*jwahn@kaist.ac.kr*

Abstract: We present a polarization shaping technique for few-cycle terahertz (THz) waves. For this, *N* femtosecond laser pulses are generated from a devised diffractive optical system made of as-many glass wedges, whcih then simultaneously illuminate on various angular positions of a sub-wavelength circular pattern of an indium arsenide thin film, to produce a THz wave of tailor-made polarization state given as a superposition of *N* linearly-polarized THz pulses. By properly arranging the orientation and thickness of the glass wedges, which determine the polarization and its timing of the constituent THz pulses, we sucessfully generate THz waves of various unconventioal polarization states, such as polarization rotation and alternation between circular polarization states.

OCIS codes: (050.1970) Diffractive optics; (320.5540) Pulse shaping; (300.6495) Spectroscopy, terahertz.

References and links

1. W. S. Warren, "Effects of pulse shaping in laser spectroscopy and nuclear magnetic resonance," Science **242,** 878–884 (1988).
2. D. Meshulach and Y. Silberberg, "Coherent quantum control of two-photon transitions by a femtosecond laser pulse," Nature **396,** 239–242 (1998).
3. A. V. Kimel, A. Kirilyuk, A. Tsvetkov, R. V. Pisarev, and Th. Rasing, "Laser-induced ultrafast spin reorientation in the antiferromagnet $TmFeO_3$," Nature **429,** 850–853 (2004).
4. T. Brixner and G. Gerber, "Femtosecond polarization pulse shaping," Opt. Lett. **26**, 557–559 (2001).
5. A. V. Kimel, A. Kirilyuk, F. Hansteen, R. V Pisarev, and Th. Rasing, "Nonthermal optical control of magnetism and ultrafast laser- induced spin dynamics in solids," J. Phys. Condens. Matter **19,** 043201 (2007).
6. M. Shapiro and P. Brumer, "Controlled photon induced symmetry breaking: chiral molecular products from achiral precursors," J. Chem. Phys. **95**, 8658–8661 (1991).
7. P. H. Siegel, "Terahertz technology," IEEE Trans. Microwave Theory Tech. **50,** 910–928 (2002).
8. M. Tonouchi, "Cutting-edge terahertz technology," Nat. Photonics **1,** 97–105 (2007).
9. J. Kono, "Spintronics: Coherent terahertz control," Nat. Photonics **5,** 5–6 (2011).
10. T. Kampfrath, A. Sell, G. Klatt, A. Pashkin1, S. Mahrlein, T. Dekorsy, M. Wolf, M. Fiebig, A. Leitenstorfer, and R. Huber, "Coherent terahertz control of antiferromagnetic spin waves," Nat. Photonics **5,** 31–34 (2011).
11. L. A. Nafie, "Infrared and Raman vibrational optical activity: theoretical and experimental aspects," Annu. Rev. Phys. Chem. **48,** 357–386 (1997).
12. R. Piesiewicz, T. Kleine-Ostmann, D. Mittleman, M. Koch, J. Schoebel, N. Krumbholz, and T. Kürner, "Short-range ultra-broadband terahertz communications: concepts and perspectives," IEEE Antennas Propag. Mag. **49,** 24–39 (2007).
13. R. Shimano, H. Nishimura, and T. Sato, "Frequency tunable circular polarization control of terahertz radiation," Jpn. J. Appl. Phys. **44**, 676–678 (2005).
14. Y. Hirota, R. Hattori, M. Tani, and M. Hangyo, "Polarization modulation of terahertz electromagnetic radiation by four-contact photoconductive antenna," Opt. Express **14,** 4486–4493 (2006).

#164860 - $15.00 USD Received 30 Mar 2012; revised 14 May 2012; accepted 14 May 2012; published 17 May 2012

15. J. Shan, J. I. Dadap, and T. F. Heinz, "Circularly polarized light in the single-cycle limit: the nature of highly polychromatic radiation of defined polarization," Opt. Express **17,** 7431–7439 (2009).
16. J. Masson and G. Gallot, "Terahertz achromatic quarter-wave plate," Opt. Lett. **31,** 265–267 (2006).
17. G. Klatt, F. Hilser, W. Qiao, M. Beck, R. Gebs, A. Bartels, K. Huska, U. Lemmer, G. Bastian, M. B. Johnston, M. Fischer, J. Faist, and T. Dekorsy, "Terahertz emission from lateral photo-Dember currents," Opt. Express **18,** 4939–4947 (2010).
18. R. N. Bracewell, *The Fourier Transform and Its Applications*, 3rd ed. (McGraw-Hill, N.Y., 2000), Ch. 13.
19. E. Hecht, *Optics*, 4th ed. (Addison Wesley, 2002), Ch. 8.
20. T. Brixner, "Poincaré representation of polarization-shaped femtosecond laser pulses," Appl. Phys. B **76,** 531–540 (2007).
21. M. Yi, K. Lee, J. Lim, Y. Hong, Y.-D. Jho, and J. Ahn, "Terahertz waves emitted from an optical Fiber," Opt. Express **18,** 13693–13699 (2010).
22. G. Matthäus, S. Nolte, R. Hohmuth, M. Voitsch, W. Richter, B. Pradarutti, S. Riehemann, G. Notni, and A. Tünnermann, "Microlens coupled interdigital photoconductive switch," Appl. Phys. Lett. **93,** 091110 (2008).
23. Y. Kim, J. Ahn, B. G. Kim, and D. Yee, "Terahertz birefringence in zinc oxide," Jpn. J. Appl. Phys. **50,** 030203 (2011).
24. J. W. Goodman, *Introduction to Fourier Optics*, 3rd ed. (Roberts & Company Publishers, Englewood, 2005), Ch. 5.
25. G. P. Wakeham and K. A. Nelson, "Dual-echelon single-shot femtosecond spectroscopy," Opt. Lett. **25,** 505–507 (2000).
26. K. Y. Kim, B. Yellampalle, A. J. Taylor, G. Rodriguez, and J. H. Glownia, "Single-shot terahertz pulse characterization via two-dimensional electro-optic imaging with dual echelons," Opt. Lett. **32,** 1968–1970 (2007).

1. Introduction

Ultrafast pulse shaping technique has enabled on-demand generation of visible light of arbitrary waveforms, making significant contributions in many research areas including laser spectroscopy [1], quantum control of non-linear processes [2], and magnetic spin state control [3], to list a few. Among the many degrees of freedom of light, polarization has been the least under consideration. In recent years, however, polarization has gradually become an important control parameter, and the polarization state shaping of optical frequency wave, which has been pursued with the help of well-developed optical devices and components, such as optical gratings, or liquid crystal devices [4], is succesfully applied for spintronics [5] and photo-biochemistry [6].

What about THz frequency wave? Recently, this undeveloped frequency region has attracted a great deal of interest [7, 8]. THz frequency waves of controlled polarization state are relevant in use for many fundamental studies. For example, the material waves of which the frequency belongs to THz region include the spin wave of magnetic materials and the vibrational waves of circularly dichroic biological molecules [9–11]. Additionally THz-frequency communication is another attractive issue, where the polarization synthesis may play an as important role as in radio-frequency communications [12]. There have been attempts to achieve the circular polarization of THz frequency waves by combining a couple of linearly-polarized THz waves [13]; or by passive optical components, such as prisms [14], Fresnel rhombs [15], achromatic wave plates [16]. Yet, the scope of THz-version of polarization state shaping is rather limitted to a few simple polarization states.

In this paper, we present an idea of polarization state shaping for arbitrary waveform synthesis for THz frequency waves, inspired by the recent work carried out by Klatt and coworkers [17]. According to their report, the photo-Dember current injected by a femtosecond laser pulse that illuminates on a metal-semiconductor interface flows perpedicular to the interface, and, as a result, the THz wave radiated in the direction of the surface normal is linearly-polarized, perpendicular to the direction of the interface. We can then use a circular interface betweem the semiconductor and metal to generate THz wave linearly-polarized along an arbitrary direction. With this method, then multiple THz waves simultaneously generated from different locations of the circular interface can be superposed to make a polarization shaped THz wave.

#164860 - $15.00 USD Received 30 Mar 2012; revised 14 May 2012; accepted 14 May 2012; published 17 May 2012

In the subsequent sections, after introducing a new definition for the polarization state of few-cycle THz pulses, we present an experimental demonstration of THz polarization synthesis technique. Diffractive optical systems are devised being made of N glass wedges ($N = 4$ or 6), which are used to produce the proprely arranged as-many optical pulses in time and space. When a femtosecond laser pulse passes through one of the diffractive optical systems, a set of laser pulses arranged in time and space is produced, which then illuminates a sub-wavelength InAs thin film to produce THz waves of tailor-made polarization states. After the proof-of-principle experiments, a short discuss of the validity of this polarization shaping technique follows.

2. Polarization representation for few-cycle THz waves

The nature of the polarization of few-cycle or sub-cycle waves differs from the well-known behavior of monochromatic or quasi-monochromatic waves [15]. As such extremely short pulses consist of a broad range of spectral components, the slowly-varying envelope approximation, which is the presumption for the conventional polarization representations, including Jones vector, Stokes vector, and Poincaré sphere representations, is not adequate. Note that the Jones vector representation uses the phase delay between two linear polarization components, defined as a function of a carrier frequency; and that the principal axes and the polarization ellipticity in Poincaré representation make no sense if the polarization changes significantly in one cycle of oscillation.

In order to properly describe the polarization state of a few-cycle pulse, therefore, a new definition for polarization ellipticity is needed, without relying on the slowly-varying envelope approximation and strictly given in terms of its constituent linear-polarization components in time domain. In mathematics and signal processing, the analytic, or time-varying complex, representation of a real-valued function facilitates the time dependence of otherwise time-invariant physical parameters, such as amplitude, phase and frequency, etc [18]. Suppose a time-varying electric field is given as a superposition of two orthogonal fields, $\hat{x}E_x(t)$ and $\hat{y}E_y(t)$, linearly polarized along the x- and y-axes, respectively. We may then define their complex field amplitudes $\tilde{E}_{x,y}(t)$ using the so-called analytic signal representation,

$$\tilde{E}_{x,y}(t) = E_{x,y}(t) + iH[E_{x,y}(t)], \tag{1}$$

where $H[E_{x,y}(t)]$ are the Hilbert transformation of $E_{x,y}(t)$ given as

$$H(E(t)) = \frac{1}{\pi} P \int_{-\infty}^{\infty} \frac{E(t')}{t-t'} dt', \tag{2}$$

where P denotes the Cauchi principal calculation. Then, the amplitudes of its right-circularly polarizated component, $\tilde{E}_R(t)$, and of its left-circularly polarized component, $\tilde{E}_L(t)$ are given as

$$\tilde{E}_{R,L}(t) = \frac{1}{\sqrt{2}} \left(\tilde{E}_x(t) \pm i\tilde{E}_y(t) \right), . \tag{3}$$

These defined parameters satisfy $\tilde{E}_x(t)\hat{x} + \tilde{E}_y(t)\hat{y} = \tilde{E}_R(t)\hat{R} + \tilde{E}_L(t)\hat{L}$ where the resulting unit vectors $\hat{R} = (\hat{x} - i\hat{y})/\sqrt{2}$ and $\hat{L} = (\hat{x} + i\hat{y})/\sqrt{2}$ denote the right- and left-circular polarizations, respectively, as in Johns vector representation [19].

In Poincaré sphere representation [20], the angle of polarization ellipticity is detemined by the ratio of the semi-major and semi-minor axes of an electrical field ellipse. For a monochromatic wave, the semi-major axis is the sum of the absolute values of the right- and left-circular polarization amplitudes, and the semi-minor axis is the difference between them. In this regard,

#164860 - $15.00 USD Received 30 Mar 2012; revised 14 May 2012; accepted 14 May 2012; published 17 May 2012

we may newly define the polarization ellipticity ε without a loss of generality as

$$\varepsilon(t) = \tan^{-1} \frac{\left|\tilde{E}_L(t)\right| - \left|\tilde{E}_R(t)\right|}{\left|\tilde{E}_L(t)\right| + \left|\tilde{E}_R(t)\right|}, \tag{4}$$

instead of using semi-major and semi-minor axes. This definition of the polarization ellipticity ε can be further simplified as,

$$\varepsilon(t) = \tan^{-1} \frac{\left|\tilde{E}_L(t)\right|}{\left|\tilde{E}_R(t)\right|} - \frac{\pi}{4}, \tag{5}$$

so ε is in fact the ratio of the right- and left-circular polarization amplitudes.

To examine the nature of the polarization state change, we consider a polarization shaped THz pulse, given as a sum of two orthogonally polarized half-cycle pulses, as

$$\vec{E}(t) = \hat{y}e^{-(t-t_1)^2/\tau^2} + \hat{x}e^{-(t-t_2)^2/\tau^2}, \tag{6}$$

where τ is the gaussian pulse duration, t_1 and t_2 are the time delays of the pulses. For simplicity, $\tau = 1$ ps, $t_1 = 3$ ps, and $t_2 = 4$ ps are chosen. Figure 1(a) shows the numerical calculation for the temporall profile and the polarization state chage of the shaped THz pulse, which shows that the electric field starts being polarized along the *y*-axis, becomes left-circularly polarized, and ends being linearly polarized along the *x*-axis.

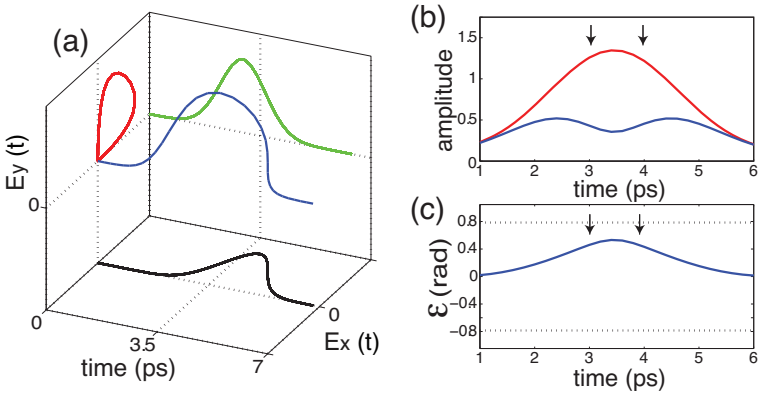

Fig. 1. (Color online) (a) Two half-cycle pulses of mutually orthogonal polarizations overlapped with a 1-ps time delay. (a) The temporal profile of the combined pulse (blue) represented in a three-dimensioal coordinate space of E_x, and E_y; and its projections to each plane, respectively. (b) The temporal profiles of the right (blue) and the left (red) circular polarization amplitudes. (c) Calculated time-varying polarization ellipticity. (For the definition, see the text.) The arrows in (b) and (c) represent the peak positions of the individual half-cycle pulses.

The polarization amplitudes $\left|\tilde{E}_R(t)\right|$ (blue) and $\left|\tilde{E}_L(t)\right|$ (red), are drawn in Fig. 1(b), and the polarization ellipticity in Fig. 1(c). The results confirms that the polarization state changes sequentially from linear, left-circular, and back to linear polarization states.

3. Experimental description

Experiments were performed in a THz time-domain spectroscopy setup. The laser source was a Ti:sapphire laser oscillator which produced 100-fs pulses at a repetition rate of 100 MHz, and

#164860 - $15.00 USD Received 30 Mar 2012; revised 14 May 2012; accepted 14 May 2012; published 17 May 2012

the central wavelength was 840 nm. The laser pulses were illuminated on an InAs thin film to generate THz pulses, as shown in Fig. 2. For the generation of polarization-shaped THz pulses, a disk-pattern of the InAs film was used. The InAs disk pattern was fabricated similarly to our previous work [21]. The (100)-oriented InAs thin film was grown by molecular beam epitaxy on AlAsSb buffered GaAs substrates. The grown InAs film and the AlAsSb buffer thicknesses were 900 nm and 2200 nm, respectively. Before the substrate was etched, we deposited the metallic hole pattern on the InAs thin film by photolithography and lift-off process for this present work. The diameter of the disk was 200 μm, and the laser spot of 5 μm diamter on its circular edge acted like a THz single point generator at the far-field. For THz detection, a microlens-coupled interdigital photoconductive antenna (PCA) was used [22]. Both the *x* and *y* polarization components were measured by rotating the PCA, as the PCA itself is capable of polarization sensitive detection [23].

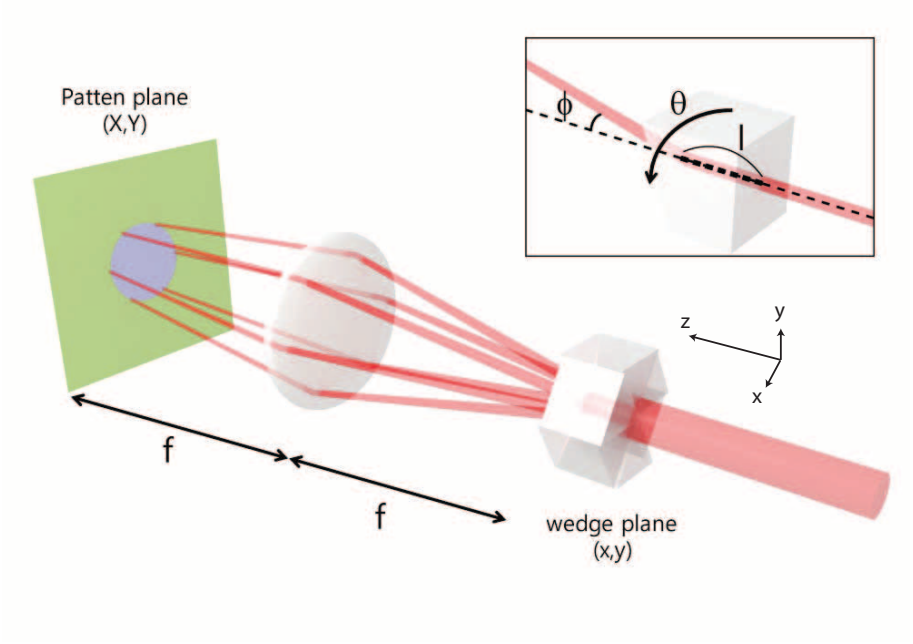

Fig. 2. (Color online) Experimental setup for the generation of polarization-shaped THz waves. (Inset) Laser beam is refracted from a single glass wedge to the edge of an InAs disk pattern, where the azimuthal angle θ and the thickness l of the glass wedge determine the polarization and timing of the generated THz pulse, respectively. When a set of glass wedges of different azimuthal angles and thicknesses is used at the same time, as-many THz pulses are generated simultaneously from the various locations in the InAs disk and the combined THz wave is made with time-varying polarization.

In order to deliver the laser beams of each power of 15 μW on specific angular locations of the InAs disk edge, we have devised a diffractive optical system made of a set of glass wedges. From a single edge, for example, a collimated laser beam is diverted, as shown in an inset figure of Fig. 2, to an angle $\phi = \sin^{-1}(n\sin\alpha) - \alpha$, where n is the index of reflection and α is the apex angle of the glass wedge, and focused by a trasform lens of focal length f. Then, the laser intensity at the InAs film plane (X,Y) is given by

$$I'(X,Y) = |\int\int \sqrt{I(x,y)}w(x,y)e^{-i\frac{k}{f}(xX+yY)}dxdy|^2, \quad (7)$$

#164860 - $15.00 USD Received 30 Mar 2012; revised 14 May 2012; accepted 14 May 2012; published 17 May 2012

where $I(x,y)$ is the laser intensity at the wedge plane, $w(x,y)$ is the spatial phase modulation induced by the wedge, and k is the propagation constant [24]. The spatial phase modulation $w(x,y)$ is given by

$$w(x,y) = e^{ik\sin\phi(x\cos\theta + y\sin\theta)}, \tag{8}$$

where θ is the azumuthal angle of the wedge, and Eq. (7) becomes

$$I'(X,Y) = |\int\int \sqrt{I(x,y)} e^{-i\frac{k}{f}[x(X-X_w)+y(Y-Y_w)]} dxdy|^2, \tag{9}$$

where $(X_w, Y_w) = (f\sin\phi\cos\theta, f\sin\phi\sin\theta)$. Therefore, the laser beam is focused at (X_w, Y_w) in the InAs flim.

In our experiments, $f = 12$ mm and $\phi = 0.5^\circ$ were used to satisfy $f\sin\phi = d/2$, where d was the diameter of the InAs disk. Therefore, as a function of the angle θ of the glass wedge, the laser beam was directed to the angular spot $(X,Y) = d/2(\cos\theta, \sin\theta)$ on the edge of the InAs disk. For the laser spot small enough compared to the InAs disk, the photo-Dember current flew generated perpendicularly to the hole edge in the plane, and the emitted THz field $E(t)$ was polarized along the direction of θ, as

$$\vec{E}(t) = \hat{\theta} E_{\text{one}}(t), \tag{10}$$

where $\hat{\theta} = \hat{x}\cos\theta + \hat{y}\sin\theta$, and $E_{\text{one}}(t)$ is the electric field time trace of a single THz pulse emitted by a laser spot on the InAs film. As $\hat{\theta}$ was changed from $0^\circ - 360^\circ$ by rotating the glass wedge, an arbitrary direction for a linearly polarized THz field was obtained.

For the generation of a complex polarization state of a THz pulse, multiple glass wedges were used as shown Fig. 2. We used two sets of multiple glass wedges, 4 and 6, in our experiment. The four different angular positions at $\theta = 0^\circ$, 90°, 180°, and 270° were illuminated by using a set of four glass wedges, or the six different angular positions among $\theta = 0^\circ - 360^\circ$ with $\Delta\theta = 60^\circ$ by six glass wedges. All the glass wedges induced the same diversion angle ϕ, and the beam through each glass wedge was temporally delayed by each additional glass plate of thickness. Note that similar temporal separation techniques have been used elsewhere, for example, the echelon techniques for femtosecond pump probe spectroscopy [25] and single shot THz time domain spectroscopy [26]. In our technique, however, spatial control by glass wedge refraction was included and laser beam was focused to N different spatial locations $(d/2\cos\theta_n, d/2\sin\theta_n)$, for $n = 1 - N$, with different timing $t_n = (n_w - 1)l_n/c$, where n_w and l_n are the refractive index and the thicknes, respectively, of the glass wedges, and c is the speed of light. The resulted THz field is given as a sum $E_{\text{total}}(t)$ that can be written as

$$E_{\text{total}}(t) = \sum_{n=1}^{N} \hat{\theta}_n E_{one}(t - t_n), \tag{11}$$

and, by properly choosing each $\hat{\theta}_n$ and t_n, a number of THz pulses of distinct polarization state were synthesized.

4. Results and discussion

First, we check the polarization linearity of a simple THz pulse as a function of the azimuthal angle θ of a single glass wedge. Figure 3 shows the measured result: the peak amplitudes of the THz pulse measured along the two orthogonal linear polarization directions, x and y, are plotted as a function of θ, in Figs. 3(a) and 3(b), respectively. Their peak amplitudes show the sinusoidal behaviors of $\cos\theta$ and $\sin\theta$, respectively, as shown in Fig. 3(c), and the calculated polarization angle shows linear to the azimuthal angle θ of the glass wedge, as in Fig. 3(d). So,

#164860 - $15.00 USD Received 30 Mar 2012; revised 14 May 2012; accepted 14 May 2012; published 17 May 2012

the polarization vector becomes $\hat{\theta} = \hat{x}\cos\theta + \hat{y}\sin\theta$, as expected in Eq. (10). For the numerical simulation, we have used a numerial fit to the single THz waveform measured in Fig. 3(e), with a function of $E_{\text{one}}(t) = c_1 \exp[-t^2/c_2^2] - c_3 \exp[-(t-c_4)^2/c_5^2]$, where $c_{1,2,\cdots,5}$ are fitting parameters.

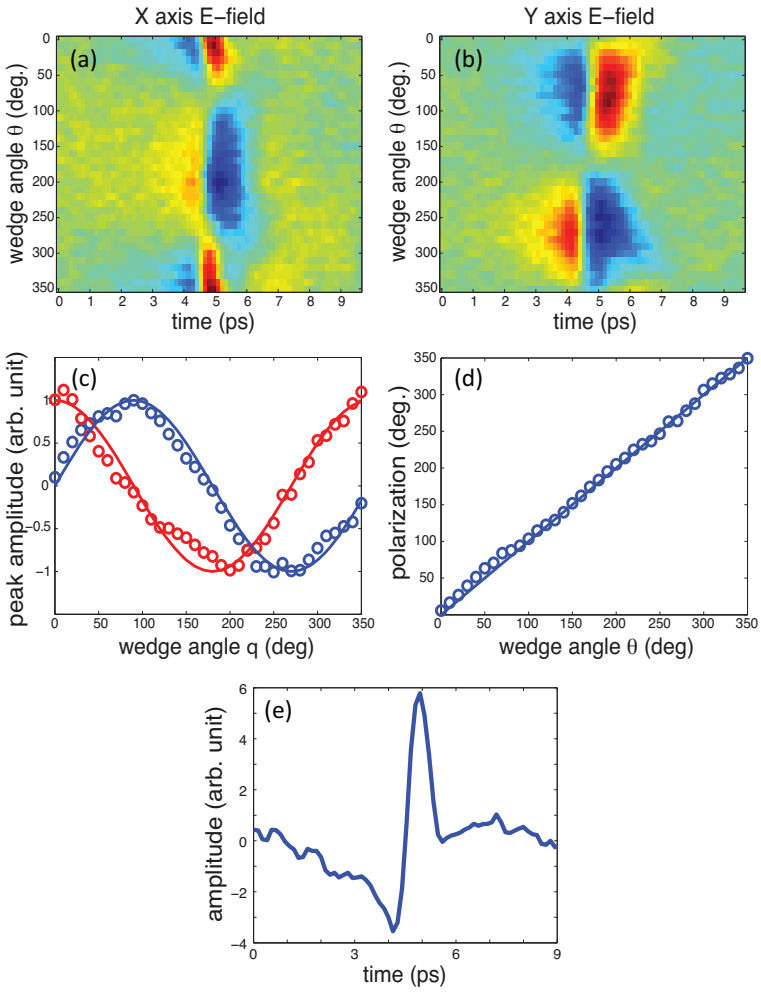

Fig. 3. (Color online) Electric filed $\vec{E}(t)$ of a linearly-polarized THz pulse measured by a polarization-sensitive detector as a function of the azimuthal angle θ of a glass wedge: (a) The measured x-polarized component, $\hat{x}\cdot\vec{E}(t)$; (b) The measured y-polarization component, $\hat{y}\cdot\vec{E}(t)$; (c) The the THz peak amplitudes of (b) and (c) plotted as a function of θ, where the dotted lines are $\cos\theta$ (red) and $\sin\theta$ (blue); (d) The polarization angle $\tan^{-1}[\hat{x}\cdot\vec{E}(t)/\hat{y}\cdot\vec{E}(t)]$ calculated from (c); (e) Time-domain waveform of a single linearly-polarized THz pulse.

Figure 4 shows the result of a four-glass wedge experiment. The four different THz pulses were overlapped in time, with individual linear polarization direction and of individual time delay. So, a polarization shaped THz wave was generated, as shown in Fig. 4(a). Along the propagation direction, the electric field vector rotated about $3\pi/2$ angle in radian. The thickness and the azimuthal angle of each glass wedge were chosen as (l_n, θ_n) = (3 mm, 270°), (4 mm, 0°),

#164860 - $15.00 USD Received 30 Mar 2012; revised 14 May 2012; accepted 14 May 2012; published 17 May 2012

(5 mm, 90°), and (6 mm, 180°), respectively, in serial order as drawn in the inset of Fig. 4(a). With this arrangement of the glass wedges, the delay times and the polarization directions of the individual THz pulses are given as (t_n, $\hat{\theta}_n$) = (1.5 ps, -$\hat{y}$), (3.0 ps, $\hat{x}$), (4.5 ps, $\hat{y}$), and (6 ps, -$\hat{x}$), respectively. The resulting THz wave (blue) is plotted in Fig. 4(a), along with the three projections to the *x*-polarization (black) and the *y*-polarization (green), and their parametric (red) planes, where the dots represent the experimental result and the lines the simulation. Figure 4(b) shows the amplitude absolute of the left- and right-circular polarizaton components, $\left|\tilde{E}_R(t)\right|$ and $\left|\tilde{E}_L(t)\right|$, respectively, as defined in Eq. (3). The polarization ellipticity is plotted in Fig. 4(c). The polarization rotation of the generated THz wave is less than 2π, so defining the ellipticity based on the principal axis of Poincaré representation may be inadequeate. Instead, we use the ellipticity parameter $\varepsilon(t)$, defined in the Eq. (4), to describe the polarization change. The dots in Fig. 4(c) denote the experimental data and the solid line the simulation, which shows that the THz wave began with linear polarization, gradually varied its polarization, and ended back to a wave of linear polarization.

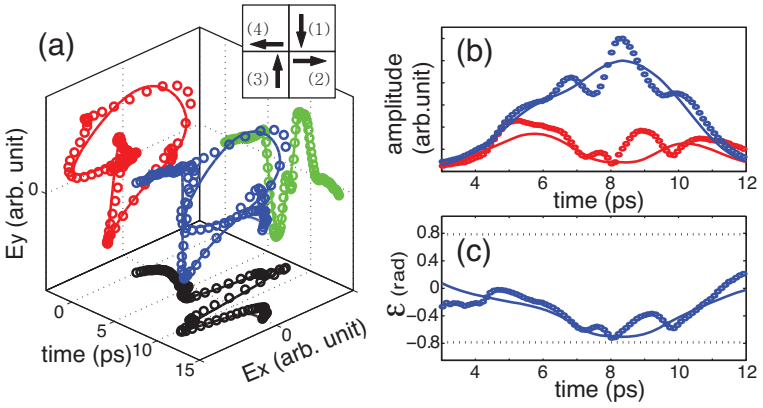

Fig. 4. (Color online) (a) THz pulse shaping with four glass wedges. The inset shows the orientation of the glass wedges. (For the detail, see the text.) Four THz pulses which are linearly polarized are weaved to make circularly polarized THz wave. (b) Calculated right-circular polarization amplitude $\left|\tilde{E}_R(t)\right|$ (blue) and left-circular polarization amplitude $\left|\tilde{E}_L(t)\right|$ (Red). (c) Calculated polarization elipticity $\varepsilon(t)$. The dotts represent the experimental data and the solid line the numerical simulation. The dashed lines along $\varepsilon(t) = \pm\pi/2$ indicate perfect circular polarization.

Figure 5 shows the result of a six-glass wedge experiment. In this experiment, six glass wedges with thickness of 3, 3.6, 4.2, 4.8, 5.4, and 6 mm, respectively, were used, and their time delays were given as t_n are $t_n = n \times 0.9$ ps for $n = 1$ to 6. Two types of time-varying polarization states were made, with two sets of glass wegde arrangements, as shown in the insets of Figs. 5(a) and 5(d), where the direction of the arrows represents the azimuthal angle θ_n and the number in the parentheses represents the thickness ordering *n* of the glass wedges. In the first example shown in Figs. 5(a)–5(c), the azimuthal angles were given as $\theta_n = 270°$, 330°, 30°, 90°, 150°, 210° for $n = 1$ to 6 (from the first to the last). With this arrangement, the polarization unit vectors $\hat{\theta}_n$ were $\hat{\theta}_1 = -\hat{y}$, $\hat{\theta}_2 = (\sqrt{3}\hat{x} - \hat{y})/2$, $\hat{\theta}_3 = (\sqrt{3}\hat{x} + \hat{y})/2$, $\hat{\theta}_4 = \hat{y}$, $\hat{\theta}_5 = (-\sqrt{3}\hat{x} + \hat{y})/2$, $\hat{\theta}_6 = -(\sqrt{3}\hat{x} - \hat{y})/2$. As a result, the polarization state evolved in time from linear, right circular, and back to linear. The next example is shown in Figs. 5(d)–5(f). In this case, the glass wedges were arranged with $\theta_n = 270°$, 30°, 150°, 210°, 90°, 330°, as shown in the inset of Fig. 5(d), and their thickness was the same as the above case. Then, the polarization direction of the constituent single THz pulses were given as $\hat{\theta}_1 = -\hat{y}$, $\hat{\theta}_2 = (\sqrt{3}\hat{x} + \hat{y})/2$, $\hat{\theta}_3 = (-\sqrt{3}\hat{x} + \hat{y})/2$,

#164860 - $15.00 USD Received 30 Mar 2012; revised 14 May 2012; accepted 14 May 2012; published 17 May 2012

$\hat{\theta}_4 = (-\sqrt{3}\hat{x} - \hat{y})/2$, $\hat{\theta}_5 = \hat{y}$, $\hat{\theta}_6 = (\sqrt{3}\hat{x} - \hat{y})/2$. The measured electric field, the calculated amplitude absolutes of the left- and right-circular polarization components, and the polarization ellipticity are shown in Figs. 5(d)–5(f), respectively. With this arrangement of glass wedges, the polarization state alternates between the right- and left-circularly polarizations. The discrepancy between the calculation and experimental results is mainly contributed from the fact that the assumption of the independence of $E_{one}(t)$s in Eq. (11) from the angle θ_n was not exactly true in the experiment. There were laser power variations for different angular positions of the InAs disk and their alignment along the disk edge were not perfect.

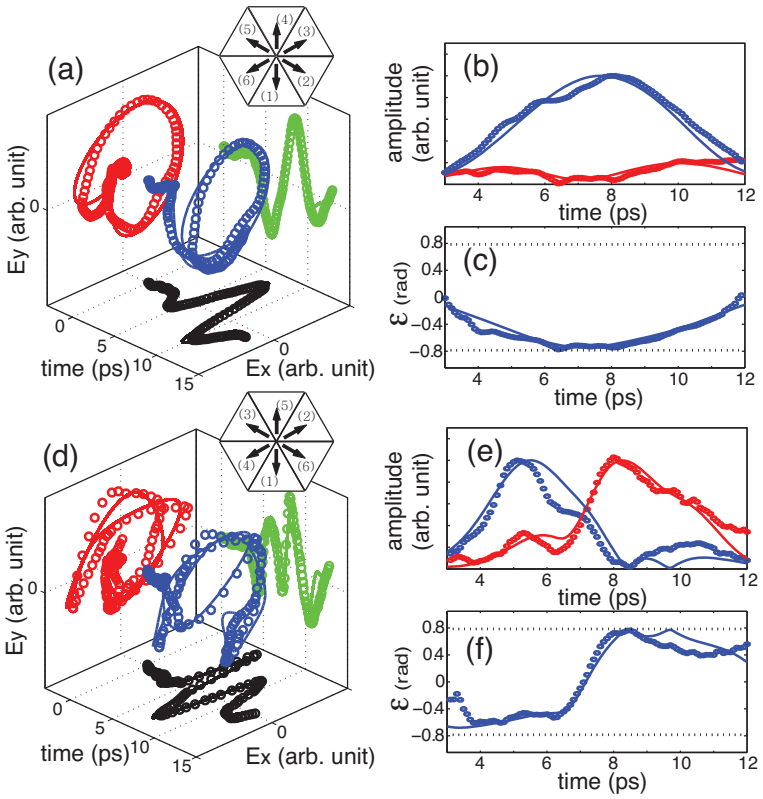

Fig. 5. (Color online) Examples of THz pulse shaping with six glass wedges. (a-c) THz pulse shaping for polarization rotation: (a) The electric field $\vec{E}(t)$ is plotted in a three-dimensional space defined by E_x, E_y, and time. The dots represent the experimental data while the solid line the simulation. The inset shows the glass wedge arrangement, where the arrows indicate the glass wedge orientation, and the ordering number indicates the glass thickeess. (b) Amplitude absolutes of the calculated right- and left-circular polarization components, $|\tilde{E}_R(t)|$ (blue) and $|\tilde{E}_L(t)|$ (red), respectively. (c) Polarization ellipticity $\varepsilon(t)$, which shows that polarization changes from linear, right-circular, and back to linear in one-cycle time duration. The dashed line at $\varepsilon(t) = \pi/2$ (-$\pi/2$) indicates perfect left (right) circular polarization state. (d-f) THz pulse shaping for polarization alternation: (d) Electric field vector, (e) circular polarization ampltude absolutes, (f) polarization ellipticity. Polarization state changes from right circular to left circular.

Now we discuss the validity of the presented THz polarization shaping technique. The arrangement of N laser pulses on as-many angular positions of the circular edge of a small InAs disk becomes technically valid if the laser spot size becomes significantly smaller than the the

#164860 - $15.00 USD Received 30 Mar 2012; revised 14 May 2012; accepted 14 May 2012; published 17 May 2012

radius of the InAs disk pattern. So, the maximum number of wedges is determined by the relation between the size of focused laser spot and the geometrical factors of the glass wedges. Suppose that the glass wedges are of a square shape of length L, which is the maximally allowed size for incoming laser beam. Then, the lateral size d of the laser spot is given by,

$$d = \frac{2f\lambda}{L}, \tag{12}$$

where λ is the wavelength of the femtosecond laser. In our experimental condition, $d \approx 0.02\ \mathrm{mm}^2/L$. Considering the size of the InAs pattern, that is $D = 200\ \mu$m, and the validity condition, $D \gg d$, we can estimate that the number of allowed angular positions for the focused laser spots, given approximately as A/L^2, where A is the lens area, reaches up to a few hundreds. Therefore, a few hudreds of glass wedges could be used in the THz pulse shaping method.

It is also worth to discuss about a proper size for the InAs pattern. If the diameter of the pattern D is increased, the experimental condition easily follows the postulation that femtosecond laser spots should be much smaller then the pattern size. However, at the same time, the spatial distribution of the THz emission points gets increased, causing an amplitude loss of the resulting net THz wave. For an estimation, we use Fourier optics theory to estimate this loss η, which is given by

$$\eta = 1 - \frac{2J_1(\pi f_{\#} D/2\lambda_{THz})}{\pi f_{\#} D/2\lambda_{THz}} \tag{13}$$

where J_1 is the first-order Bessel function of the first kind, λ_{THz} is the wavelength of the THz wave, and $f_{\#}$ is the f-number of its focusing optics. In our experiment, $f_{\#}$ =1, and the amplitude loss ratio is estimated less then 10% for the most part of the frequency range of the generated THz waves. If we used a circular pattern with D = 600 μm, a 30% amplitude loss at 0.5 THz is expected.

5. Summary

In summary, we have presented a THz pulse shaping technique for polarization state control, by superposing a number of THz pulses of various linear polarization vectors. For this, a number of femtosecond optical pulses were arranged spatially and temporally with a set of glass wedges of various thickness, and were used to illuminate on various angular locations of the circular edge of a InAs disk pattern. Then, the lateral photo-Dember currents off from the edge interface generated linearly polarized THz pulses, whose polarization direction was determined by the direction of the currents. For experimental demonstration, we used two systems made of four or six glass wedges to synthesize various unconventioal polarization states, such as polarization rotation and alternation between circular polarization states.

Acknowledgments

This work was supported in part by Basic Science Research Programs [2009-0090843, 2010-0013899, 2009-0083512] and in part by the World Class Institute Program [WCI 2011-001] through the National Research Foundation of Korea funded by the Ministry of Education, Science and Technology of Korea.

#164860 - $15.00 USD Received 30 Mar 2012; revised 14 May 2012; accepted 14 May 2012; published 17 May 2012